Growth of thin Pd, Fe, Co and Ag films on A1 single crystal surfaces
by Nagarajah Rajamohan Shivaparan

A thesis submitted in partial fulfillment of the requirements for the degree of Doctor of Philosophy in Physics
Montana State University

Abstract:
The objective of this study was to investigate the formation of intermetallic compounds at the interface between surfaces of Al single crystals and various metal overlayers; also, to identify the fundamental physical parameters which determine the atomic structure of these interfaces.

The growth of thin Pd, Fe, Co and Ag films on Al(001) and Al(110) surfaces at room temperature was studied using high-energy ion scattering (HEIS), x-ray photoelectron spectroscopy (XPS) and low-energy electron diffraction (LEED). For Pd deposited on Al(110) surfaces, a strong Pd-Al mixing occurs at the Pd-Al interface. The interface mixing was observed to continue up to about 10 monolayers (ML) of Pd coverage, at which point the intermixing stops. XPS measurements of the Pd 3d photopeaks show a chemical shift that is consistent with the formation of an Pd-Al like compound at the interface and the growth of Pd metal thereafter.

Similar results were observed in the cases of Fe and Co on Al(001) and Al(110) surfaces. Deposited Fe atoms seem to intermix with the substrate Al atoms up to about 5 ML and 9 ML coverages of Fe on Al(001) and Al(001) surfaces respectively. A Volmer-Weber type growth model was used to identify the phases formed at the interfaces for both surfaces. On the other hand, Co atoms deposited on Al(001) and Al(110) surfaces. seem to displace the substrate Al atoms up to about 3ML and 5ML respectively. Based on the XPS intensity analysis we conclude that the CoAl phase was formed at the interface with near "surface" dechanneling at the interface. On the Al(001) surface, a very diffuse LEED pattern with high background intensity was observed after a deposition of 7.6 ML of Co coverage. The LEED pattern never came back on the Al(110) surface even after 15 ML of Co deposition.

In contrast to the above mentioned transition metals, Ag deposited on the Al(001) and Al(110) surface seemed to grow in an epitaxial overlayer at room temperature. XPS intensity curves and LEED strongly support the idea that the growth mode of Ag atoms on the Al(001) surface cannot be simply layer-by-layer but rather a formation of clusters of Ag atoms. On the other hand, deposited Ag atoms seem to grow layer-by-layer on the Al(110) surface.

Finally, it has been observed that the growth mode of deposited metal atoms on Al surfaces is not correctly predicted by the aluminide formation energy or the lattice mismatch. Instead, using a model for surface strain in forming the surface alloy, we found that the size of the overlayer atom compared to the substrate Al atom correlates well with the growth behavior for metals on Al surfaces.

GROWTH OF THIN Pd, Fe, Co AND Ag FILMS ON Al SINGLE CRYSTAL SURFACES

by

Nagarajah Rajamohan Shivaparan

A thesis submitted in partial fulfillment
of the requirements for the degree

of

Doctor of Philosophy

in

Physics

MONTANA STATE UNIVERSITY-BOZEMAN
Bozeman, Montana

November 1996

APPROVAL

of a thesis submitted by

Nagarajah R. Shivaparan

This thesis has been read by each member of the thesis committee, and has been found to be satisfactory regarding content, English usage, format, citations, bibliographic style, and consistency, and is ready for submission to the College of Graduate Studies.

Richard J. Smith — Richard J Smith (Signature) — 11-27-96 Date

Approved for the Department of Physics

John C. Hermanson — J Herm (Signature) — 11-27-96 Date

Approved for the College of Graduate Studies

Robert L. Brown — R L Brown (Signature) — 12/3/96 Date

STATEMENT OF PERMISSION TO USE

In presenting this thesis in partial fulfillment of the requirements for a doctoral degree at Montana State University-Bozeman, I agree that the Library shall make it available to borrowers under rules of the Library. I further agree that copying of this thesis is allowable only for scholarly purposes, consistent with "fair use" as prescribed in the U.S Copyright Law. Requests for extensive copying or reproduction of this thesis should be referred to University Microfilms International, 300 North Zeeb Road, Ann Arbor, Michigan 48106, to whom I have granted "the exclusive right to reproduce and distribute my dissertation in and from microfilm along with the non-exclusive right to reproduce and distribute my abstract in any format in whole or in part".

Signature N. R. Bly

Date 11/27/96

To my late grandfather ***Karthigesu Sinnathurai***,

and

To my **parents** and **family members**, who have given their unqualified love, understanding, and support throughout my life.....

ACKNOWLEDGEMENTS

It is my pleasure to acknowledge the persons who have helped me complete this endeavor. First and foremost, I wish to thank my adviser, Prof. Richard J. Smith, for his great care and patience, gentle nudging and nurturing, and his boundless, infectious enthusiasm. Truly, it has been "fun".

I also wish to express my sincere gratitude to Eric Anderson and Norm Williams for their patience and invaluable help in carrying out various aspects of this work. I really owe them a big one.

Special thanks go to Prof. Gerald J. Lapeyre and Asst. Prof. Lisa D. Peterson for their valuable advice and continuous assistance throughout my research.

In addition, several of my colleagues helped immeasurably. Adli A. Saleh, V. Shutthanandan, Volker Krasemann, Marcus Teter, and many others contributed in countless ways.

I gratefully acknowledge the support of the Physics Department and the National Science Foundation throughout my stay here.

Finally, to my parents, brothers, and sisters, go the greatest praise. They supported me in so many ways. Financially, emotionally, spiritually. I know it was hard to put up with my prolonged absences, both physical and mental. To them go my utmost heartfelt thanks and love.

N.R.Shivaparan, November, 1996.

TABLE OF CONTENTS

LIST OF TABLES

LIST OF FIGURES

ABSTRACT

The objective of this study was to investigate the formation of intermetallic compounds at the interface between surfaces of Al single crystals and various metal overlayers; also, to identify the fundamental physical parameters which determine the atomic structure of these interfaces.

The growth of thin Pd, Fe, Co and Ag films on Al(001) and Al(110) surfaces at room temperature was studied using high-energy ion scattering (HEIS), x-ray photoelectron spectroscopy (XPS) and low-energy electron diffraction (LEED). For Pd deposited on Al(110) surfaces, a strong Pd-Al mixing occurs at the Pd-Al interface. The interface mixing was observed to continue up to about 10 monolayers (ML) of Pd coverage, at which point the intermixing stops. XPS measurements of the Pd 3d photopeaks show a chemical shift that is consistent with the formation of an Pd-Al like compound at the interface and the growth of Pd metal thereafter.

Similar results were observed in the cases of Fe and Co on Al(001) and Al(110) surfaces. Deposited Fe atoms seem to intermix with the substrate Al atoms up to about 5 ML and 9 ML coverages of Fe on Al(001) and Al(110) surfaces respectively. A Volmer-Weber type growth model was used to identify the phases formed at the interfaces for both surfaces. On the other hand, Co atoms deposited on Al(001) and Al(110) surfaces seem to displace the substrate Al atoms up to about 3ML and 5ML respectively. Based on the XPS intensity analysis we conclude that the CoAl phase was formed at the interface with near "surface" dechanneling at the interface. On the Al(001) surface, a very diffuse LEED pattern with high background intensity was observed after a deposition of 7.6 ML of Co coverage. The LEED pattern never came back on the Al(110) surface even after 15 ML of Co deposition.

In contrast to the above mentioned transition metals, Ag deposited on the Al(001) and Al(110) surface seemed to grow in an epitaxial overlayer at room temperature. XPS intensity curves and LEED strongly support the idea that the growth mode of Ag atoms on the Al(001) surface cannot be simply layer-by-layer but rather a formation of clusters of Ag atoms. On the other hand, deposited Ag atoms seem to grow layer-by-layer on the Al(110) surface.

Finally, it has been observed that the growth mode of deposited metal atoms on Al surfaces is not correctly predicted by the aluminide formation energy or the lattice mismatch. Instead, using a model for surface strain in forming the surface alloy, we found that the size of the overlayer atom compared to the substrate Al atom correlates well with the growth behavior for metals on Al surfaces.

CHAPTER 1

INTRODUCTION

The behavior of the outer atomic layer of a surface and its interaction with atoms or molecules of adsorbates is the cornerstone of surface science. A complete understanding, at the atomic level, of these fundamental interactions would have important technological spin-offs, since they are crucial to all surface chemical reactions, catalysis and thin film nucleation[1]. It is important not only to determine the elements of species involved, but also their molecular structure and orientation. At this level, highly specific experiments are required using techniques dedicated to the full characterization of a model system, usually comprising a single crystal substrate and a well defined adsorbate species. This has become more practical with improvements in our capabilities using ultrahigh vacuum technology. Yet, we are still lacking a comprehensive model which can be used to predict the atomic structure at a metal-metal interface.

We have focused our investigations on transition-metal-aluminum (TM-Al) bilayers, and formation of transition-metal aluminides because of the technological importance of these materials. In particular, several of the TM-aluminides have potential applications as metallization layers in III-V semiconductor devices, as demonstrated recently for CoAl and NiAl on GaAs[2,3] and FeAl on InP[4]. Another technology that will benefit from studies of the TM-Al interface is concerned with the fabrication of thin-film magnets, where controlling the atomic structure could be important for designing the magnetic properties of the film. Also, thin films of transition metal aluminides may have

different physical properties than those of the bulk material since the electronic and atomic structures in the overlayer may also be modified. Palladium, for example, shows an enhanced magnetic susceptibility associated with the expansion of the Pd unit cell in the Au-Pd-Au epitaxial structure.[5] Finally, we expect that the models developed during our investigations for predicting and characterizing epitaxial growth and surface alloy formation will be generally applicable to the case of metal-on-metal growth.

At this point it is useful to spend some time in understanding the factors which determine the epitaxial growth of one material on another. First of all, the term "*epitaxy*" (Greek) means the "*growth of crystals on a crystalline substrate that determines their orientation*". Until about 1960, most theoretical approaches to the problem were based on the concept of a small misfit (lattice mismatch). Royer, who coined the term epitaxy[6], used x-ray diffraction to demonstrate that such oriented growth requires that lattice planes in both materials have similar structure. He concluded that epitaxial growth requires a misfit ε ($\varepsilon = |b-a|/a$, where a and b are the in-plane lattice constants of substrate and overlayer) of not more than about 15%. However, there are many important cases where the epitaxial layer has a totally different crystal structure (e.g., silicon on sapphire[7], CdTe on sapphire[8]). For such systems, the above criterion of lattice match is no longer applicable. Therefore a good lattice match is never a sufficient condition for epitaxial growth. We may hope, however, that the converse is true, namely that certain film faces will not grow as single crystals on a given substrate because of a poor lattice match.

Some other important parameters involved in determining epitaxial growth are substrate temperature, substrate orientation, deposition rate of adatoms, heat of formation, size of the adatom and the strain introduced by the overlayer. In general, the quantity which determines the growth mode may be written in simplified form as $\Delta = \sigma_f + \sigma_i - \sigma_s$, where σ_f and σ_s are the specific surface free energies of film and substrate, respectively, and σ_i the specific free interfacial energy[9]. Three modes of thin film growth are frequently observed, namely, the Volmer-Weber mode (3D crystals) results when $\Delta > 0$, and the Frank- van der Merwe (FM) and the Stranski-Krastanov (SK) modes when $\Delta \leq 0$. For the FM (monolayer by monolayer) mode to occur, the condition $\Delta \leq 0$ must be fulfilled for each layer h: $\Delta_h \leq 0$. In general, the condition $\Delta \leq 0$ can be fulfilled for only one or a few monolayers so that the SK mode (3D crystals on top of one or a few monolayers) will prevail. Depending upon the variation of Δ_h with h and of σ_i with the size and shape of the island in the h^{th} layer, transitions between the two modes may occur.

This thesis work is part of an ongoing investigation to understand the fundamentals which we discussed above to determine the growth modes of ultrathin transition metal films deposited on Al single crystal surfaces at room temperature. From our previous studies of Ti on Al(110) and Al(001) surfaces[10], we found that Ti films grow epitaxially up to a critical thickness, after which the growth mode changes in character. On the other hand, Ni films mix with the Al surface to form a surface alloy[11].

In this thesis work we explored the growth of ultrathin Pd films on Al(110) surfaces, and Fe, Co and Ag films on Al(001) and Al(110) surfaces. During the growth

process, the atomic structures of the overlayer and the substrate were monitored using different surface science techniques. In summary, we found that neither the aluminide formation energy, nor the lattice mismatch alone serve as useful parameters to predict epitaxial growth. Instead the relative size of the adatoms correlates well with the growth behavior for transition metals (Ti, Ni, Pd, Co and Fe) on Al surfaces as discussed in the summary section. The adatom size dependence was further tested using Ag which has a larger atomic diameter than the Al substrate atom.

In Chapter 2, the basic theory of the techniques that we used is briefly reviewed. The experimental setups and procedures are discussed in detail in Chapter 3. A combination of complementary surface science techniques was used to verify the initial state of the clean and ordered Al surfaces. These techniques were also used to monitor the growth of the deposited films at various stages of the experiment. The primary technique, high energy ion scattering (HEIS), along with x-ray photoelectron spectroscopy (XPS), and low energy electron diffraction (LEED) were used in this thesis work. In chapters 4, 5, 6 and 7, the results of ultrathin Pd, Fe, Co and Ag films deposited on Al surfaces are reported. The results of Chapters 4 and 5 have been published in Surface Science[12,13]. The results of Chapters 6 and 7 will be submitted for publication in the near future.

The following is a list of acronyms frequently used in this thesis:

AES	Auger electron spectroscopy
FAT	Fixed-analyzer transmission
FM	Frank-van der Merwe

FWHM	Full width at half maximum
HA	Hemispherical analyzer
HEIS	High energy ion scattering
LEED	Low energy electron diffraction
MC	Monte Carlo
MCA	Multichannel analyzer
MCS	Multichannel scaling
ML	Monolayer
PIPS	Passivated, implanted, planner silicon detector
PHA	Pulse height analysis
RBS	Rutherford backscattering spectrometry
RGA	Residual gas analyzer
SPA	Surface peak area
SK	Stranski-Krastanov
UHV	Ultra high vacuum
VEGAS	Ion scattering simulation program
VW	Volmer-Weber
XPS	X-ray photoelectron spectroscopy
XPD	X-ray photoelectron diffraction

REFERENCES

1. Surface Science techniques, edited by J. M. Walls and R. Smith, Pergamon, Elsevier Science, Inc., New York, 1994.

2. M. Tanaka, N. Ikarashi, H. Sakaibara, K. Ishida and T. Nishinaga, Appl. Phys. Lett. 60, (1992) 835.

3. S. A. Chambers, J. Vac. Sci. Technol. B 7, (1989) 737.

4. A. M. Wowchak, J. N. Kuznia and P. I. Cohen, J. Vac. Sci. Technol. B 7, (1989) 733.

5. M. B. Brodsky and A. J. Freeman, Phys. Rev. Lett. 45, (1980) 133.

6. L. Royer, Bull. Soc. Fr. Mineral. Crist. 51 (1928) 7.

7. G. W. Cullen, in Heteroepitaxial Semiconductors for Electronic Devices, edited by G. W. Cullen and C. C. Wang (Springer, New York, 1978).

8. T. H. Myers, Y. Cheng, R. N. Bicknell, and J. F. Schetzina, Appl. Phys. Lett. 42, (1983) 247.

9. E. Bauer, Appl. of. Surf. Sci., 11/12, (1982) 479.

10. Adli A. Saleh, Ph.D Thesis, Montana State University, 1994.

11. V. Shutthanandan, Ph.D Thesis, Montana State University, 1994.

12. N. R. Shivaparan, V. Shutthanandan, V. Krasemann and R. J. Smith, Surf. Science, in press.

13. N. R. Shivaparan, V. Krasemann, V. Shutthanandan and R. J. Smith, Surf. Sci., 365, (1996) 78.

CHAPTER 2

SHORT REVIEW OF THEORIES

Introduction

The experimental techniques used in this thesis work are high-energy ion scattering (HEIS), channeling, X-ray photoelectron spectroscopy (XPS), and low energy electron diffraction (LEED). The primary work has been measurement of the surface peak area (SPA) of the substrate (Al) and the adsorbate (Pd, Fe, Co, and Ag) in HEIS at different adsorbate coverages in order to investigate the behavior and growth modes of ultrathin transition metal films deposited on Al-single crystal surfaces. Furthermore, HEIS was used to measure the actual coverage of the adsorbate. In addition, XPS measurements have been performed to identify the chemical state of the reacted transition metal-Al interface during the adsorbate deposition. Also, LEED measurements have been used to perform surface crystallography including the atomic structure, epitaxial growth, the periodicity of atoms, and the overall symmetry of the surface, but not the detailed atomic positions. In this chapter we give a brief description of physical concepts and the theory behind these powerful surface science techniques. In the next chapter we will discuss the instrumentation and the experimental details of these techniques.

High-energy Ion Scattering and Channeling

It is well known that many chemical and electronic properties of surfaces and interfaces are related to the atomic structure at the surface or interfaces such that investigations of the surface and interface structure become more and more important. Rutherford Backscattering Spectroscopy (RBS) is a commonly used, non-destructive, surface analysis probe for structure determination in modern physics.[1,2,3] RBS has also proved to be a useful tool for in-depth analysis of thin film composition and structure. RBS spectra are straightforward to interpret because of the simple, classical nature of the ion-solid interaction. Considerable surface sensitivity is achieved when the incident ion beam is aligned along a low index crystal axis.

For MeV He^+ ions, the de Broglie wavelength is of the order of 10^{-12} cm; thus the crystal lattice is not viewed as a diffraction grating but rather as an array of rows and sheets of nuclei that collimate and steer the beam. When the ion beam is aligned along a crystal axis, on the scale of interatomic distances the ion is simply a point probe weaving through the channels provided by the rows and planes of atoms. Hence, this particular RBS technique is called high-energy ion scattering/channeling.

A hypothetical RBS spectrum from a single-element target is shown in Figure 2.1. The beam of energetic He^+ ions with energy E_o, mass M_1, and charge Z_1 strikes the sample (with atomic mass M_2 and charge Z_2) at normal incidence, and backscattered ions are detected at a scattering angle θ. While a small fraction of the beam scatters from the

surface atoms, additional scattering occurs from the atoms just below the surface. In moving through a sample before the scattering is encounter and passing back out through the sample after the scattering event, the ions continuously lose energy. The ions scattered from surface atoms will reach the detector with energy KE_o, where K is a constant less than unity. The ions scattered from the atoms which are below the surface will scatter at energies less than KE_o, as shown in Figure 2.1.

In the sections that follow, the four basic physical parameters that govern the RBS process: kinematic factor, differential scattering cross section, stopping cross section and energy straggling.

Kinematic factor K

For scattering at the sample surface the only energy loss mechanism is via momentum transfer to the target atom. Figure 2.1 illustrates the scattering of energetic ions from a single-element target. The energy of the ions backscattered from the surface atoms can be related to the incident energy via the kinematic factor K:

$$E_1 = K E_o, \tag{2.1}$$

where K is given by

$$K = \left[\frac{M_1 \cos\theta + (M_2^2 - M_1^2 \sin^2\theta)^{1/2}}{(M_1 + M_2)} \right]^2 \tag{2.2}$$

Equation 2.2 shows that the kinematic factor depends only on the masses M_1 and M_2, and the scattering angle θ.[1]

Differential scattering cross section $d\sigma/d\Omega$

The relative number of particles backscattered from a target atom into a given solid angle Ω for a given number of incident particles is related to the differential scattering cross section. The probability for the scattering event to occur as illustrated in Figure 2.1 depends on the average scattering cross section σ. For a small Ω, the average scattering cross section can be approximated using the differential scattering cross section $d\sigma/d\Omega$. Moreover, if the interaction between the ions and the atoms is specified by the Moliere potential,[4] then the differential scattering cross section is given by[5]

$$\frac{d\sigma}{d\Omega} = F\left[\frac{Z_1 Z_2 e^2}{2E_o \sin^2\theta}\right]^2 \frac{\left[\left(1-\left[\frac{M_1}{M_2}\sin\theta\right]^2\right)^{1/2}+\cos\theta\right]^2}{\left[1-\left[\frac{M_1}{M_2}\sin\theta\right]^2\right]^{1/2}} \qquad (2.3)$$

where F is a screening correction factor

$$F = 1 - \frac{0.042 Z_1 Z_2{}^{4/3}}{E(keV)} \qquad (2.4)$$

Stopping cross section

Only a small fraction of the incident He ions undergo a close encounter with an atomic nucleus and are backscattered out of the sample. The vast majority of the incident He atoms end up implanted in the sample. When probing particles penetrate to some depth in a dense medium, the projectile energy dissipates due to interactions with

electrons and to glancing collisions with the nuclei of target atoms. This means that a particle which backscatters from an element at some depth in a sample will have measurably less energy than a particle which backscatters from the same element on the sample surface. The majority of energy loss is caused by electronic stopping which behaves like friction between the probing particles and the electron clouds of the target atoms. If we consider these energy losses in the solid for the ingoing and outcoming ions, then ΔE, the energy difference between ions scattered from the surface and ions scattered at a depth x from the surface, is given by[1]

$$\Delta E = x \left[\frac{K}{\cos\theta_1} \frac{dE}{dx} \Big|_{E_0} + \frac{1}{\cos\theta_2} \frac{dE}{dx} \Big|_{KE_o} \right] \tag{2.5}$$

θ_1 is defined as the angle between the surface normal of the sample and the direction of the incident ions, and θ_2 is defined as the angle between the normal direction and the direction of backscattered ions. For normal incidence, $\theta_1 = 0^\circ$ and $\theta_2 = 180^\circ - \theta$, where θ is the scattering angle in the laboratory. Energy loss dE/dx is related to the stopping cross section ε by the following equation

$$\frac{dE}{dx} = \varepsilon N, \tag{2.6}$$

where N is the atomic density of the target atoms.

Using equation 2.5 and 2.6, we can convert the energy-difference equation into a depth equation[1], i.e.,

$$\Delta E = N \, x \, [\varepsilon] \tag{2.7}$$

with

$$[\varepsilon] = \left[\frac{K}{\cos\theta_1}\varepsilon(E_o) + \frac{1}{\cos\theta_2}\varepsilon(KE_o)\right] \tag{2.8}$$

$\varepsilon(E_o)$ and $\varepsilon(KE_o)$ are evaluated at energy E_o and KE_o, respectively.

Energy straggling

After passing through a target with a finite thickness the probing He atoms will not only lose energy, but they will also no longer be monoenergetic. Instead, they will have a distribution of energies which is predicted by energy loss calculations. The process through which a probing He atom loses energy involves a large number of interactions with individual atoms along its trajectory through the sample. The trajectories differ from one particle to the next so that identical energetic particles, with the same initial velocity do not have exactly the same energy after passing through a solid medium. The variation in energy loss is called energy straggling. Furthermore, straggling sets a fundamental limit on the depth resolution possible with ion beam energy loss techniques. The majority of energy loss occurs through interaction with electrons. As a result, energy straggling increases with the atomic number of the target element, since atomic number also reflects the number of electrons present. Energy straggling causes the low energy edge of peaks to broaden. For thick, high Z materials this effect can be quite pronounced. The accuracy of depth resolution depends on how accurately the contribution of straggling can be calculated.

Scattering Yield

In backscattering measurements the total number of detected particles, or yield Y, from a thin layer of atoms, Δt, is given by

$$Y = Q\,N\,\Delta t\,\frac{d\sigma}{d\Omega}\Omega, \tag{2.9}$$

Q is the measured number of incident particles at the target,

$N\Delta t$ is the number of target atoms/cm^2 in the layer of thickness Δt with atomic density N (atoms/cm^3),

$d\sigma/d\Omega$ is the differential scattering cross section and

Ω is the solid angle subtended by the detector.

For the example illustrated in Figure 2.1, the ion scattering yield in the surface region of the sample is equal to the height H_o of the spectrum. Using equation 2.9 and 2.6, H_o

$$H_o = \frac{d\sigma(E)}{d\Omega}\Omega Q\frac{\delta E}{[\varepsilon]}, \tag{2.10}$$

where δE is the energy loss associated with thickness Δt of the sample, and is typically the energy width of a single channel in the energy distribution spectrum. The other parameters are the same as before.

Channeling

The principle of channeling can be illustrated by Figure 2.2. When a beam of ions is incident parallel to a major crystallographic axis or plane, the average electric field of the columns or planes of atoms acts to gently guide the ions down the center of the channel. The ions spiral down the axis where the electron density is at its lowest with a characteristic wavelength of a few tens of nm. The rate of energy loss is therefore less for channeled ions than for non-channeled ions, and the ions seldom come close enough to the lattice nuclei to suffer a large angle scattering event. A small fraction of the incident ions will collide with nuclei in the top plane of atoms and be scattered. However, subsequent crystal atoms will be in the shadow of the top atom and cannot contribute to the RBS yield. This is illustrated in Figure 2.3 which shows the surface interactions between the incident beam and a single crystal target. In a static representation, i.e., no thermal motion, the flux distribution of ions has a distance of closest approach to the second atom, R, within which there are no ions. Thus the small-angle forward scattered ions form a "shadow cone" with radius R_c, that extends into the solid (see Figure 2.3). For Coulomb scattering,

$$R_c = 2\sqrt{\frac{Z_1 Z_2 e^2 d}{E}} \tag{2.11}$$

For helium ions channeled down a major crystallographic axis, the RBS yield from atoms behind the first layer can be as low as 1% of that from an amorphous sample of the same material. If the ion beam is gradually directed away from the crystal axis, an angle will be

reached, known as the critical angle Ψ_c, at which the steering effect can no longer channel the beam and the RBS yield will increase. Such an angular yield curve (yield of ions as a function of the angle, Ψ, between the incident ion beam and symmetry direction of the crystal) is illustrated in Figure 2.4. For helium ions, the width of the angular yield curve $\Psi_{1/2}$ lies typically within the range 0.3 to 1.2°. It can be calculated using the following equation:[7]

$$\Psi_{1/2} = 0.8 F_{RS}(\xi)\Psi_1 \tag{2.12}$$

where

$$\psi_1 = 0.307\ (Z_1\ Z_2/E\ d)^{1/2}\ \text{(degrees)} \tag{2.13}$$

The incident energy E is in MeV, ξ = 1.2 ρ/a (ρ is the one dimensional rms vibration amplitude and a is the Thomas-Fermi screening radius), d = 0.707 a, and F_{RS} = square root of the dimensionless string potential obtained using Moliere's screening function. For 1 MeV He^+ ions incident along the [001] direction of Al, R_C = 0.055 Å. Since the bulk value of ρ is 0.105 Å (at room temperature), the shadowing is not big enough to cover the second atom.

The reduction in the yield of backscattered ions on an Al(001) crystal is shown graphically in Figure 2.5 by comparing the spectrum for the channeled yield or aligned yield with that for the random yield. Roughly 95% of the incident He^+ ions are channeled through the crystal. Note that it is this suppression of the scattering from the bulk in the aligned spectrum that permits measurement of the surface peak and hence provides information on the surface structure. Due to the limitations of depth resolution, the

aligned yield will show a small *surface peak* (SP), spread over the first few channels of the spectrum. Random spectra can be collected when the crystal axes are tilted away from the incident beam direction so that incident particles are not channeled, and encounter nearly all of the target atoms. The yield collected in the random direction is referred to as the *random yield.*

The surface peak is a measure of surface order, while the minimum yield behind the surface peak (Figure 2.5) is a measure of the bulk crystal perfection. In addition, a measure of the channeling effect is the quantity $\chi_{min,}=Y_A/Y_R$, defined as the ratio of the aligned to random yield. This minimum yield can be calculated from the relation[7]

$$\chi_{\min} = Nd\pi(2u_1^2 + a^2) \qquad (2.14)$$

where N is the atomic density, u_1 is the atomic one dimensional thermal vibrational amplitude, d is the interatomic distance along the row, and a is the Thomas-Fermi screening radius. Values of χ_{min} are typically between 1% and 4%. The value of χ_{min} from Fig. 2.5 is 3.6%.

In Figure 2.5 the surface peak area (SPA) is a direct measure of how many surface atoms are visible to the incident ion beam. Thus if we know the SPA (yield Y), Q, Ω and the differential scattering cross section, then by using Equation 2.9 we can calculate the product NΔt, the number of atoms per unit area visible to the incident beam.

Ion channeling is also well suited to study overlayer/substrate interactions[1]. Figure 2.6 demonstrates five simple cases of how this technique can be utilized in surface studies and shows the corresponding surface peak spectra. Fig. 2.6(a) represents

the scattering yield from a crystal with an ideal surface for the case where the thermal vibration amplitude ρ is much less than the shadow cone radius R_c. This is the condition that assures that the surface peak intensity corresponds to one atom/row in this ideal case. Fig. 2.6(b), represents a situation where the second atom is not shadowed. The surface peak intensity in this case is twice that of the ideal crystal. In a number of crystals, the inter-layer separation between the surface layer and the second layer differs from the bulk layer separation. This effect is called surface relaxation. To test for relaxation, one must also use a nonnormal incidence direction, so that the shadow cone established by the surface atoms is not aligned with the atomic rows in the bulk. The normal incidence yield would still give a surface peak intensity equivalent to approximately one monolayer. These two measurements, at normal and oblique incidence, would reveal the presence of relaxation. In Fig. 2.6(d) an adsorbate atom is positioned exactly over the surface atoms (e.g in epitaxial growth) and hence shadows the surface atoms and reduces the substrate surface peak. Examples of epitaxial systems are Ti on Al[9] and Ag on Al (Chapter 7). On the other hand, an increase in the substrate peak area as a function of overlayer thickness, where the ion beam is aligned with the substrate, is indicative of mixing where the substrate atoms are displaced from their equilibrium positions as shown in Fig 2.6(e). Examples of mixing are explained in detail in Chapters 4[10] ,5[11] and 6[12]. Note that the coverage of adsorbate atoms on the surface is determined directly from the area of the surface peak for the adsorbate (shaded peaks in Fig. 5).

X-ray Photoelectron Spectroscopy

The interaction of an X-ray photon with a sample may lead to the ejection of photoelectrons, as shown schematically in Figure 2.7. This diagram illustrates the X-ray photon interacting with an electron in the K-shell, causing the emission of a 1s photoelectron. The resulting K shell vacancy is filled by an electron from a higher energy level, which can lead to either X-ray fluorescence or the radiationless de-excitation process of Auger emission. The determination of the kinetic energy of the outgoing photoelectron is the cornerstone of experimental XPS. The kinetic energy (E_k) of the ejected photoelectron is related to the electron binding energy (E_B), the parameter that defines both the element and atomic level from which it emanated, and other instrumental terms in the following manner.[8]

$$E_k = h\nu - E_B - E_R - \phi \qquad (2.15)$$

E_R is the recoil energy, a minor component of the calculation (0.1-0.01eV), which is less than other uncertainties within the expression and is generally ignored. The sample work function is represented by ϕ. As the photon energy of the X-rays ($h\nu$) and ϕ are known and E_k is determined experimentally, E_B can be determined.

A typical X-ray photoelectron spectrum is illustrated in Figure 2.8 and the various components that contribute to it are clearly evident. From the energetic positions, intensities, and in some cases the shapes of the various peaks, one can extract valuable information about the sample. Conventionally, the origin of the energy scale is taken at

the Fermi level E_F of the solid (for metals), and the energetic separation of the different peaks is denoted by their binding energies E_B. The characteristic XPS core level peaks are superimposed on a background of inelastically scattered electrons.

Element identification

X-ray photoelectron spectroscopy is a straightforward and useful technique for the identification of atomic species at the surface of a solid. From the XPS spectrum shown in Figure 2.8, we are able to identify the elements present in the surface region of the sample. Since the binding energies of each element are well defined, the peak identification of the elements in XPS spectra is straightforward. Other important information beyond simple binding energy data and element identification can also be gleaned from an XPS spectrum. For example, the spin orbit splitting can be seen in Figure 2.9, where an XPS spectrum for the Pd 3d core-level is shown.

Chemical Shifts

The concept of chemical shifts is based on the idea that the inner shell electrons feel an alteration in binding energy due to a change in the valence shell contribution to the potential, as a result of the outer electron chemical bonding. In the simplest picture, valence electrons are drawn away from or toward the nucleus depending on the type of bond. The greater the electronegativity of the surrounding atoms, the more the displacement of electronic charge from the atom and the higher the observed binding

energies of the core electrons. An example of the shift in the Al 2p XPS spectrum as a result of formation of Al_2O_3 is shown in Figure 2.10. Here the shift in the Al signal represents 2.1 eV for the transformation from Al to Al_2O_3.

Quantitative Analysis

One of the major advantages of XPS is the ease with which quantitative data can be routinely obtained. This is usually performed by determining the area under the peak (intensity) in question. The intensity of a given line depends on a number of factors including the photoelectric cross section σ, the electron escape depth λ, the spectrometer transmission, surface roughness or inhomogeneities, as well as the presence of satellite structure. A photoelectron which originates at a certain depth below the surface will lose energy through inelastic scattering events involving other electrons. Due to this energy loss, not all the photoelectrons excited from a given subshell contribute to the photopeak. The number of electrons that can escape from a solid without undergoing an elastic collision decreases with the depth x as $\exp(-x/\lambda)$, where λ is the mean free-path. Alternatively, the intensity of photoelectrons unscattered after traveling through a material of thickness x is given by the following equation.

$$I(x) = I_o \exp\left[\frac{-x}{\lambda(E_k).\cos\Theta}\right] \qquad (2.16)$$

where I_o is the photoelectron intensity at depth x, and Θ is the angle of emission with respect to the surface normal. In order to calculate the emission intensity, a proper

background subtraction should be performed in any of the original XPS spectra. There are different forms by which background can be removed, namely linear, Tougaard, and polynomial. In Appendix, the curve fitting routines used for background subtraction, and the different line shapes of the XPS peaks in this thesis work are discussed in more detail.

Low Energy Electron Diffraction

In our LEED measurements, an electron with a wavelength λ (energy 20 to 500 eV) impinges perpendicular to a periodic row of atoms with interatomic spacing *a*. Constructive interference will occur when the electron wavelets scattering from one atom are in phase with waves scattered from adjacent atoms. This situation is shown schematically in Figure 2.11.[4] In 1-D, there will be cones around the axis of the row where constructive interference can occur and where we will have a finite probability of finding the electron. A two-dimensional periodic arrangement with primitive atomic spacing *a* and *b* will generate two sets of diffraction conditions which must be met simultaneously, namely

$$n_a\lambda_a = a \sin\theta_a \qquad n_b\lambda_b = b \sin\theta_b \tag{2.17}$$

As both conditions must be met simultaneously, the only regions where we may find the electron are in the intersections of these cones. It is obvious that the intersection of two cones with a common origin will result in a set of lines. If we set a detection device

across this set of lines, we will perceive them as spots or points which are called LEED patterns. The experimental details of LEED shall be discussed in the next chapter.

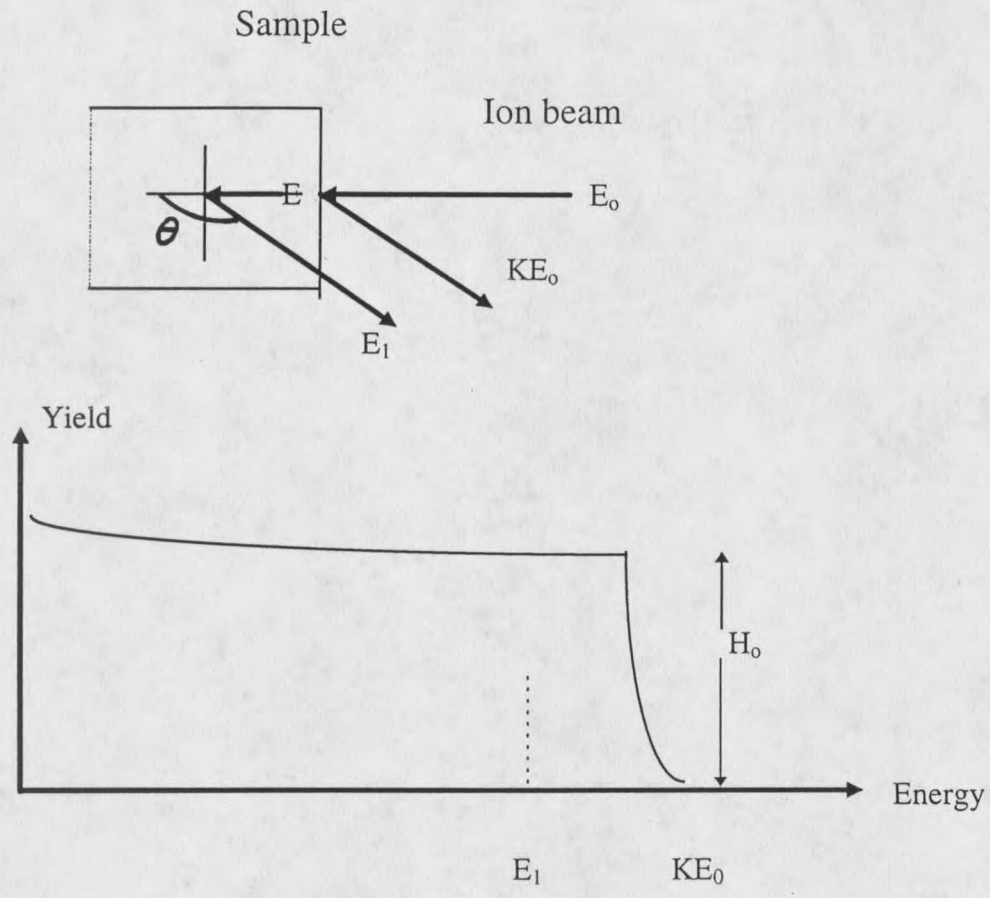

Figure 2.1: Schematic of Rutherford backscattering spectroscopy (RBS)

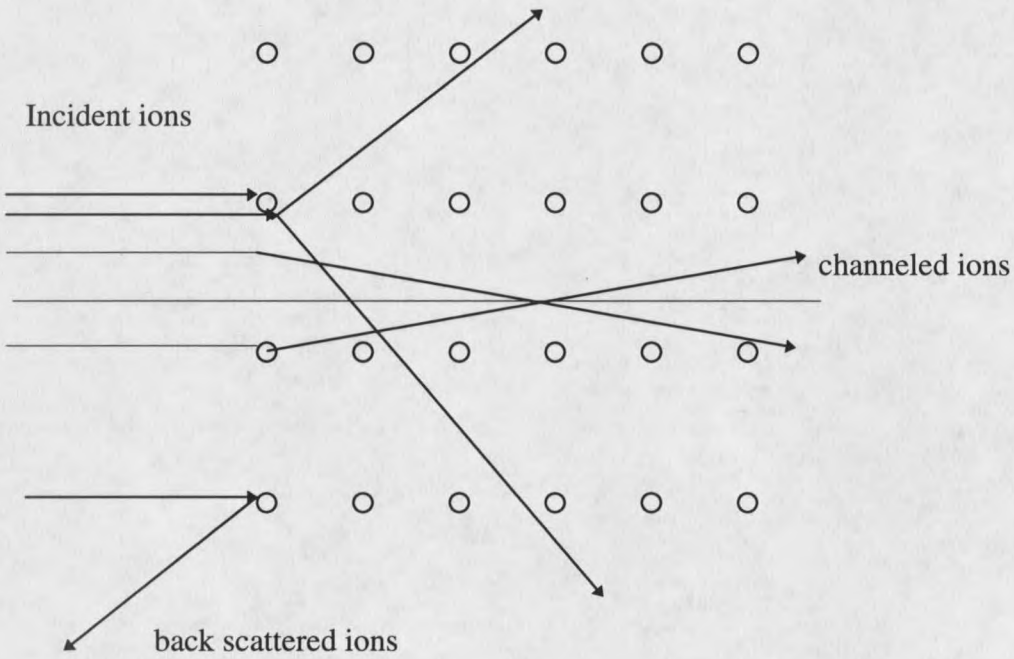

Figure 2.2: A schematic representation of possible particle paths for a beam of ions incident parallel to a crystal axis or plane.

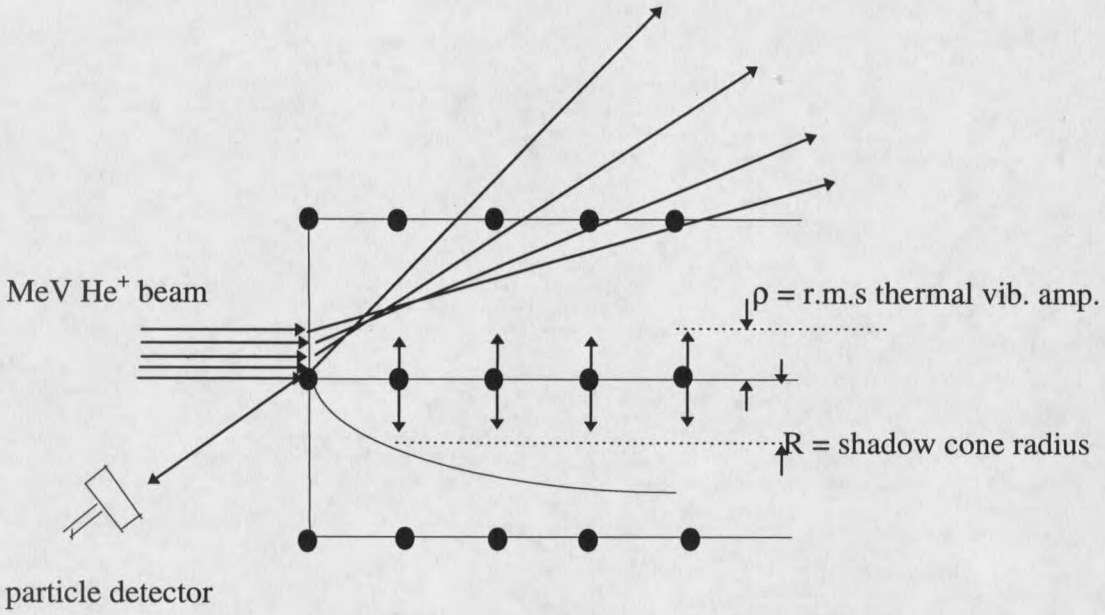

Figure 2.3: Ion trajectories near the surface of an aligned single crystal and the formation of the shadow cone.